Heliyon 10 (2024) e31849

Contents lists available at ScienceDirect

Heliyon

journal homepage: www.cell.com/heliyon

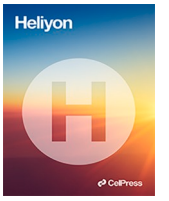

Research article

Optimization of ultra-precision CBN turning of AISI D2 using hybrid GA-RSM and Taguchi-GRA statistic tools

Amanuel Diriba Tura [a,*], Elly Ogutu Isaya [a], Ugonna Loveday Adizue [a,b], Balázs Zsolt Farkas [a], Márton Takács [a]

[a] *Budapest University of Technology and Economics, Faculty of Mechanical Engineering, Department of Manufacturing Science and Engineering, Budapest, Hungary*

[b] *Projects Development Institute (PRODA), Department of Engineering Research Development and Production, Enugu, Nigeria*

ARTICLE INFO

Keywords:
Face hard turning
Hybrid GA-RSM approaches
Taguchi-GRA statistic tools
Surface roughness
Cutting force

ABSTRACT

Ultra-precision turning is a crucial process in the manufacturing industry as it helps to produce parts with high dimensional accuracy, surface finish, and tolerance. The process is similar to traditional turning but is carried out under special circumstances to achieve greater precision and surface finish. The process can be applied to conventional structural materials, but the demand for machining hardened steels is increasing. The optimization of ultra-precision turning of AISI D2 using cubic boron nitride (CBN) tools is a crucial aspect in the field of high-quality machining. This study aims to evaluate the performance of the process and identify the optimal parameters that result in the best quality components while using a CBN tool's ultra-precision turning of AISI D2. Ultra-precision turning process factors such as cutting speed, feed, and depth of cut were experimentally investigated to enhance the response output, such as surface roughness and cutting force components. The full factorial experimental design was used for determining the process characteristics under different conditions, and experimental results were applied to search for the optimum response of machining performance. The optimization process was done by combining the hybrid genetic algorithm-response surface methodology (GA-RSM) and the Taguchi-grey relational analysis (GRA) statistical tools. These methods are useful in situations where the relationship between the input variables and the output responses is complex and non-linear. The results showed that a hybrid GA-RSM approach, combined with Taguchi-GRA statistical analysis, can effectively find optimal process parameters, leading to the best combination of surface roughness and cutting force. In hybrid Taguchi - GRA, the optimal cutting conditions were found to be a cutting speed of 175 m/min, a feed of 0.025 mm, and a depth of cut of 0.06 mm. The findings of this study provide valuable insights for the optimization of ultra-precision CBN turning operations, contribute to the development of precision manufacturing technology, and can be used as a reference for similar machining processes.

1. Introduction

Ultra-precision turning machines are specialized machines that are designed to produce highly precise and accurate parts with tight

* Corresponding author.
E-mail address: tura.amanueldiriba@edu.bme.hu (A.D. Tura).

https://doi.org/10.1016/j.heliyon.2024.e31849
Received 18 June 2023; Received in revised form 5 May 2024; Accepted 22 May 2024
Available online 23 May 2024

tolerances [1]. These machines use advanced technologies, such as computer numerical control (CNC), high-speed spindles, and precision feed systems, to achieve extremely precise cuts and finishes. Ultra-precision turning is often used in the production of parts for optical, medical, and electronic devices, as well as aerospace components, where high levels of accuracy and repeatability are required [2–4]. The process typically involves using a single-point cutting tool to remove material from a rotating workpiece while controlling the cutting tool's position and movement with high precision. The machines used for ultra-precision turning require specialized skills to operate and maintain. They are also often more expensive than traditional turning machines due to the advanced technologies and materials used in their construction. However, their ability to produce high-precision parts can lead to significant cost savings and improved product quality in many industries [5–10] Ultra-precision CBN (Cubic Boron Nitride) turning is a machining process that utilizes CBN cutting tools to produce highly accurate parts with tight tolerances and excellent surface quality [11–13].

Numerous studies have been conducted on the optimization of ultra-precision machining process utilizing various cutting tools to improve machining effectiveness, reduce machining times, and improve the surface quality and cutting force. For instance, Sizemore et al. [14] use machine learning to enhance the surface quality of the machine component while ultra-precision diamond cutting single-crystal germanium. By taking into account the tool rake angle, edge radius, cutting speed, and cutting thickness, Minghai et al. [15] investigate the effect of the strain rate during the ultra-precision turning of single-crystal silicon on the anisotropy of surface roughness. The findings of this study demonstrate that optimally uniform surface roughness may be achieved by using a lower edge radius, higher cutting rates, and a thinner cutting layer. In ultra-precision machining, Ji et al. [16] investigate the impact of grain refinement on the cutting force of metals that are challenging to work with. The findings demonstrate that following grain refining, an increase in cutting force is caused by an improvement in the stability of grain boundaries and an increase in the number of grains. In the ultra-precision turning of magnesium aluminate spinel, Geng et al. [17]investigate the impact of turning parameters and material microstructure on material removal behavior ($MgAl_2O_4$). They recommend an idealized set of turning settings to turn polycrystalline hard and brittle materials with minimum damage and a smooth surface. Through the use of finite element simulations and experimental validations, Zhang et al. [18] research reveals the machining mechanisms involved in the ultra-precision diamond micro-milling of a copper workpiece. The study focuses on the relationship between tool chatter behaviour and the shape of the machined surface. In order to produce ultra-precision single-point diamond-turning titanium alloys sustainably, Hatefi and Hossein [19] carried out an experimental examination into the impacts of magnetic field aid on the quality of the surface finish. According to the findings, magnetic field aid has demonstrated potential improvements in cutting stability and surface finish quality. In the ultra-precision machining of polar microstructures, which are employed for optical precision measurement, Zhao et al. [20] evaluated the impact of the cutting strategy on polar microstructures and the optimization of machining parameters. A series of tests and orthogonal simulations utilizing a diamond tool is used by Ruibin and Wu [21] to investigate the ultra-precision cutting process of Ti6Al4V alloy. Wanget et al. [22] investigate the impact of tool-tip vibration on surface roughness when turning copper with an ultra-precision diamond tool. Wu et al. [23] look at how tool wear affects the surface micro-topography of copper that has been turned with extreme accuracy using a diamond tool. By examining the chip formation, Schneider [24] examined the surface integrity of the titanium being cut with extreme accuracy. Nano-positioning techniques have been studied by Nam et al. [25] for use in the ultra-precision machining of Ti6Al4V alloy-based biomedical applications.

The optimization of ultra-precision CBN turning of AISI D2 steel is an important aspect to improve the process efficiency, reduce the machining time, and enhance the surface quality of the workpiece. This study aimed to optimize the ultra-precision turning of AISI D2 using a cubic boron nitride (CBN) tool by investigating the effect of various input parameters such as cutting speed (v_c), feed (f), and depth of cut (a_p) on the output responses, such as surface roughness (R_a), and cutting force (F_c). The optimization process was carried out using a hybrid of genetic algorithm-response surface methodology (GA-RSM) and Taguchi-grey relational analysis (GRA) statistical tools. This method is useful in situations where the relationship between the input variables and the output responses is complex and non-linear.

2. Experimental infrastructure and investigation methods

2.1. Experimental material

In this research, a cylindrical workpiece made of AISI D2 steel with a hardness of 62 HRC was machined. AISI D2 steel is a high carbon, high chromium alloy tool steel that is often used in punches, dies, and moulds in the manufacturing industry and is known for its excellent wear resistance and ability to hold a sharp edge. It is also commonly used in cold work tooling applications due to its high hardness and abrasion resistance [26,27] Table 1 displays the chemical makeup of the workpiece material.

Table 1
Chemical composition of AISI D2 steel.

Workpiece	Chemical composition						
	C	Si	Mn	V	Mo	Cr	Fe
AISI D2 steel	1.55	0.25	0.35	0.90	0.80	12.0	Balance

2.2. Experimental set-up

The experiments were performed using Cubic Boron Nitride (CBN) tools with cutter diameters of 0.05 m on an ultra-precision CNC machine of type of Hembrug Slentbed Mikroturn 50. The front surface of the experimental specimen was turned at a continuously variable rotational speed so that the cutting speed remained at the specified value. The cutting direction was therefore transverse to the axis of the workpiece. The experimental set-up for this inquiry is shown in Fig. 1. A Mitutoyo Stylun SJ-410 surface roughness tester was applied to measure the surface quality, which has a stylus tip diameter of up to 5 μm, a cut-off length of 0.25 mm, an X-axis measuring range of up to 120 mm × 1oomm, a resolution 0.01 μm, and 1 μm per 150 mm positioning accuracy. A dynamometer (Kistler, type 9257A) was used to measure the cutting force component (F_c) and a Kistler 9257 was applied to signal amplification. Table 2 shows the technical specifications of the ultra-precision machine used in the experiments.

2.3. Experimental design

The quality attributes of machined components are significantly influenced by process parameters, according to the literature. Examining the combined influence of machining factors on the quality attributes of the components produced was therefore crucial. As a consequence, three important process variables – cutting speed, feed, and depth of cut – each with three levels were selected as inputs for this study. As suggested by the literature review, the values of each element were modified. The process parameters that were investigated during this investigation are listed in Table 3, along with their ranges. The default values for the other parameters were kept. A total of 27 experiments were utilized, based on the full factorial experimental design, which depends on the number of input variables, and their levels as shown in Table 4. In order to increase the reliability of the results, machining with each parameter combination was repeated twice, so a total of 81 experiments were performed. The three experimental results belonging to the parameter combination were recorded and the mean value of the measured responses were calculated and used for the analysis and the optimization.

2.4. Hybrid GA-RSM optimization

Hybrid GA-RSM (Genetic Algorithm-Response Surface Method) optimization is a method of optimization that combines the strengths of both genetic algorithms (GA) and response surface method (RSM) to find the optimal solution to a problem. In GA-RSM optimization, the GA is used to generate a set of candidate solutions, also called "chromosomes", and the RSM is used to model the connection between the input variables and the output response. The GA searches the solution space using a heuristic method, while the RSM uses a mathematical model to approximate the function that relates the input variables to the output response. The hybrid GA-RSM method is particularly useful for problems with many variables or for problems that are difficult to solve using traditional optimization methods alone. This method can also be applied for problems with non-linear or non-convex constraints and for problems with multiple local optima. It is important to note that the optimization process will be highly dependent on the specific problem and the implemented hybrid method, thus, the choice of the appropriate method and tuning of the parameters is crucial for successful optimization [28–31].

2.5. Hybrid Taguchi-GRA optimization

The hybrid Taguchi-GRA optimization is a combination of two optimization methods: Taguchi method and Grey Relational Analysis (GRA). The hybrid Taguchi-GRA optimization combines the strengths of these two methods by first using the Taguchi method to identify the most important factors that affect the performance of the system and then using the GRA method to analyze the relationship between these factors and the performance of the system. The result is an optimized solution that is based on both the experimental design and statistical analysis. The hybrid Taguchi-GRA optimization method is a useful tool for engineers and

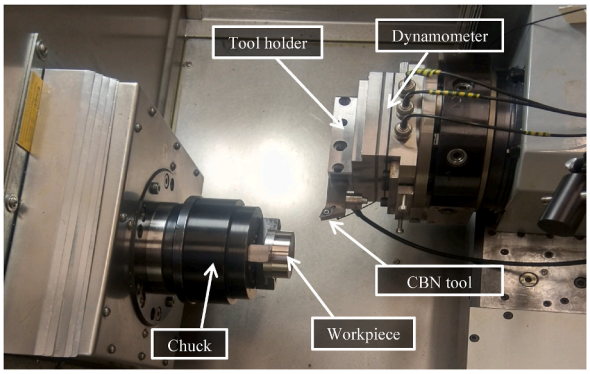

Fig. 1. Experimental set-up of the investigated ultra-precision CNC turning process.

Table 2
Technical specifications.

Hydrostatic spindle	
Spindle run-out	<0,1 μm
Spindle speed	2000 rpm −10,000 rpm
Work range	Ø 120 mm × 100 mm
Hydrostatic slides	
Rapid traverse	10 m/min
Z-axis travel	100 mm
X-axis travel	240 mm
Resolution	0,01 μm
Repeatability	±0,1 μm
Positioning accuracy	1 μm/150 mm
Siemens	840 D CNC Control

Table 3
Process parameters and their ranges for the experiments.

S. No.	Input parameters	Symbols	Units	Levels		
				Low (-1)	Medium (0)	High (+1)
1	Cutting speed	v_c	m/min	75	125	175
2	Feed	f	mm	0.025	0.075	0.125
3	Depth of cut	a_p	mm	0.06	0.08	0.1

Table 4
Full factorial experimental design matrix and measured responses.

Run Order	Machine parameters			Response	
	v_c (m/min)	f (mm)	a_p (mm)	Mean R_a (μm)	Mean F_c (N)
1	75	0.125	0.06	0.670	76.707
2	175	0.125	0.06	0.584	64.850
3	125	0.125	0.06	0.679	69.547
4	125	0.025	0.06	0.214	32.006
5	175	0.075	0.06	0.443	46.233
6	125	0.075	0.06	0.409	50.019
7	175	0.025	0.06	0.289	27.829
8	75	0.075	0.06	0.377	56.284
9	75	0.025	0.06	0.261	35.293
10	175	0.025	0.08	0.236	36.602
11	125	0.025	0.08	0.249	39.453
12	125	0.125	0.08	0.676	82.103
13	175	0.125	0.08	0.645	77.806
14	125	0.075	0.08	0.304	63.637
15	75	0.075	0.08	0.326	70.751
16	75	0.025	0.08	0.224	45.020
17	175	0.075	0.08	0.317	57.411
18	75	0.125	0.08	0.867	91.284
19	125	0.025	0.1	0.245	44.473
20	75	0.125	0.1	0.928	104.582
21	125	0.075	0.1	0.350	73.893
22	75	0.025	0.1	0.238	50.328
23	75	0.075	0.1	0.318	79.240
24	175	0.025	0.1	0.270	38.489
25	125	0.125	0.1	0.671	103.624
26	175	0.125	0.1	0.676	96.204
27	175	0.075	0.1	0.360	66.533

researchers who are working to improve the performance of a product or process. It can be applied to a wide range of problems, including product design, process optimization, and system optimization [32–39]. Fig. 2 shows the overall flow methodology used in this research.

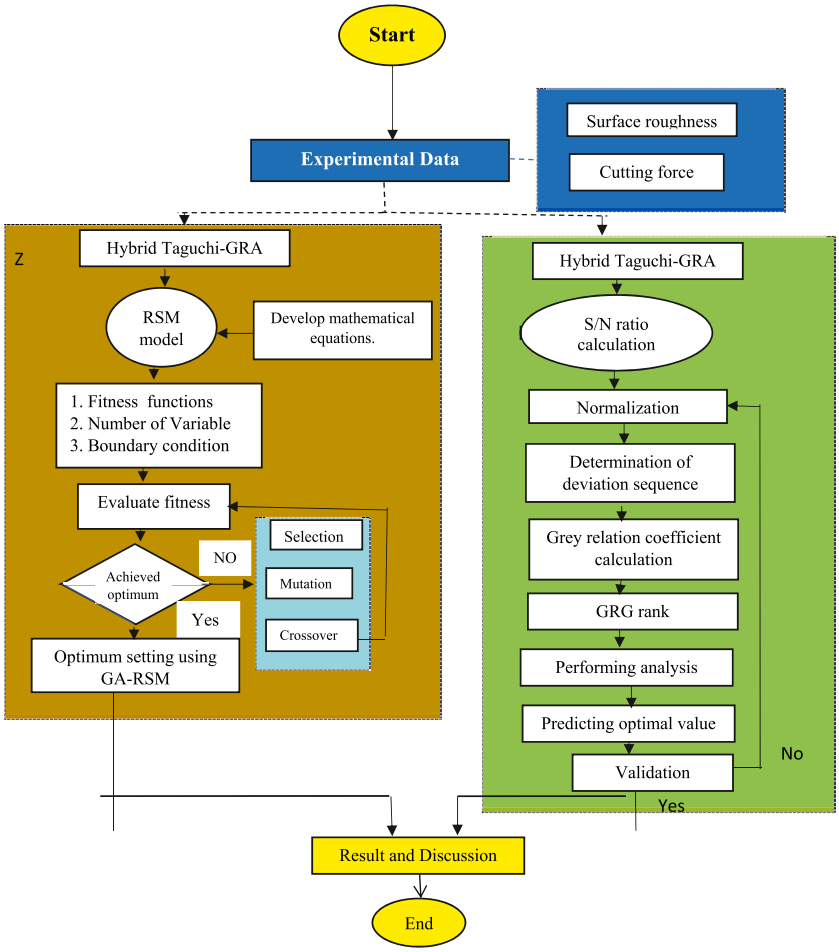

Fig. 2. Flow methodology chart proposed in the research.

3. Results and discussion

3.1. Impact of input parameters

The experimental outputs of R_a and F_c were investigated using Taguchi analysis, main effect plots, and a pie chart plot to investigate the influence of process parameters. Taguchi analysis was done in Minitab V18 by setting small to be the best R_a and F_c, and it shows the ranking of various factors in terms of their relative importance to the relative changes in R_a (Table 5) and cutting force (Table 6). It's observed from Table 4 that feed is the most important factor affecting R_a, followed by cutting speed and depth of cut. Feed is the most significant factor impacting F_c, followed by the depth of cut and cutting speed, as shown in Table 5.

The importance of the input parameters can also be evaluated based on the contour plots. Fig. 3(a)-(c) and Fig. 4(a)-(c) show the variation of the mean R_a and F_c with the input parameters, respectively. Mean R_a was considerably influenced by feed, but cutting speed had a negligible effect, as shown by the contour plot in Fig. 3(a)–and a lower mean R_a was achieved at the lower feed. According to Fig. 3(b), the lower Ra values were obtained between 0.07 mm and 0.09-mm depth of cut, and cutting speed had little to no effect on mean Ra. As can be seen in Fig. 3(c), the mean Ra was not significantly impacted by the cut depth. The results showed that between

Table 5
Taguchi analysis for R_a.

Level	Cutting speed (m/min)	Feed (mm)	Depth of cut (mm)
1	0.4677	0.2473	0.4362
2	0.4219	0.3560	0.4271
3	0.4244	0.7107	0.4507
Delta	0.0458	0.4633	0.0236
Rank	2	1	3

Table 6
Taguchi analysis for F_c.

Level	Cutting speed (m/min)	Feed (mm)	Depth of cut (mm)
1	67.72	38.83	50.97
2	62.08	62.67	62.67
3	56.88	85.19	73.04
Delta	10.84	46.36	22.07
Rank	3	1	2

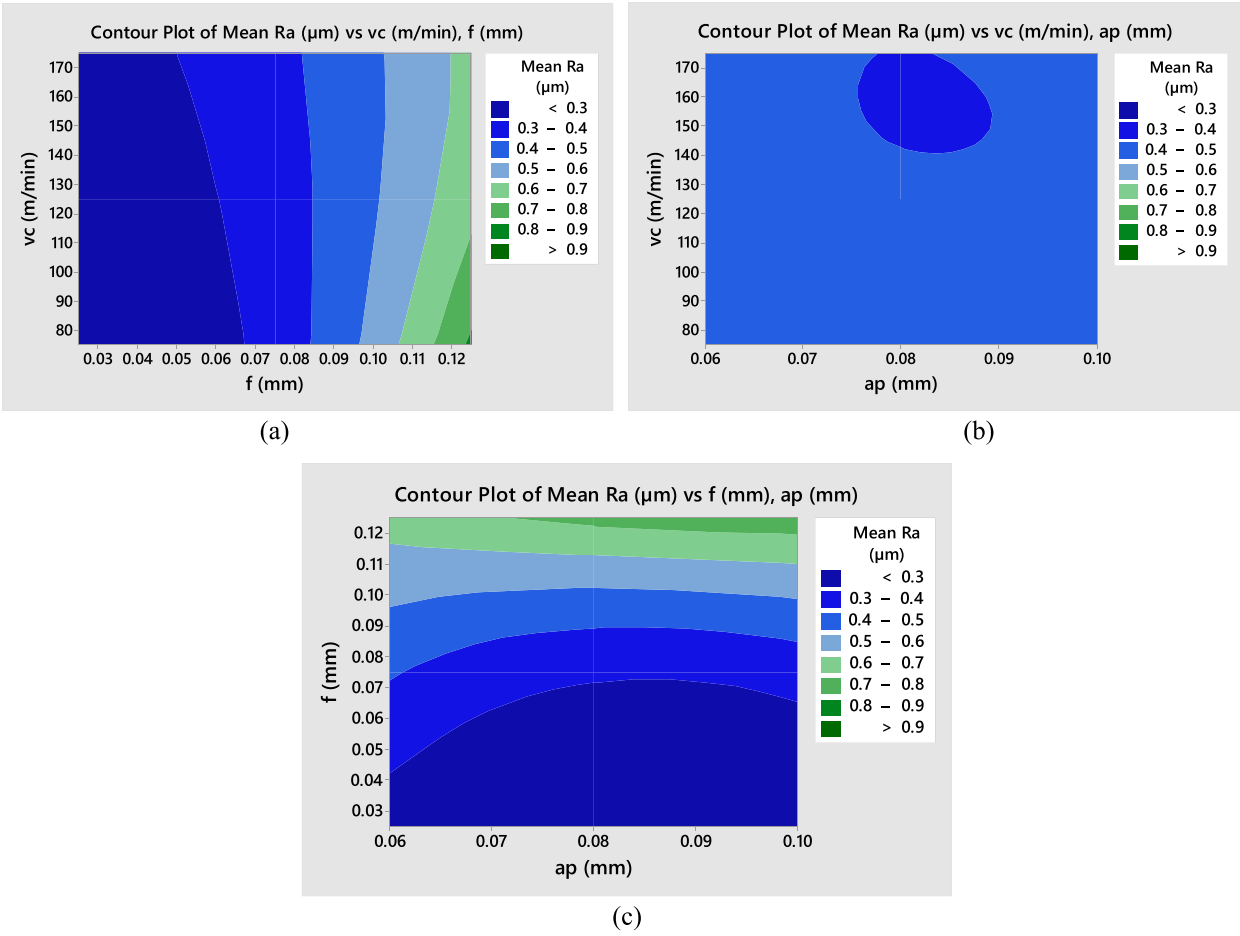

Fig. 3. Contour plot of (a) R_a and (b) F_c with all process parameters.

0.03 mm and 0.05 mm feed, between 80 and 100 m/min cutting speed, and between 0.07 and 0.09 mm cut depth, a lower mean Ra was obtained.

Fig. 4(a) shows that lower mean F_c is achieved with lower feed and higher cutting speed, and feed has a dynamic effect on mean F_c. A lower mean F_c was observed at the lower levels of depth of cut and feed, as shown in Fig. 4(b). A lower mean F_c objected to a lower cutting speed and depth of cut, as seen in Fig. 4(c). The findings demonstrate that decreased mean F_c demands resulted in objections to decreased cutting rates, feeds, and cut depths. Additionally, it shows that feed, followed by cutting speed and depth of cut, significantly influence the mean F_c.

3.2. Multi-objective optimization of process response using hybrid GA-RSM

3.2.1. Developing regression models using RSM

In this study, regression mathematical equations were developed using experimental data and Minitab v18 software to account for the connection between the process variables' R_a and F_c. The presented mathematical equations may be used with any combination of machining parameters to approximate experimental findings for R_a and F_c by using variables with a prob > F below 0.05. The results of

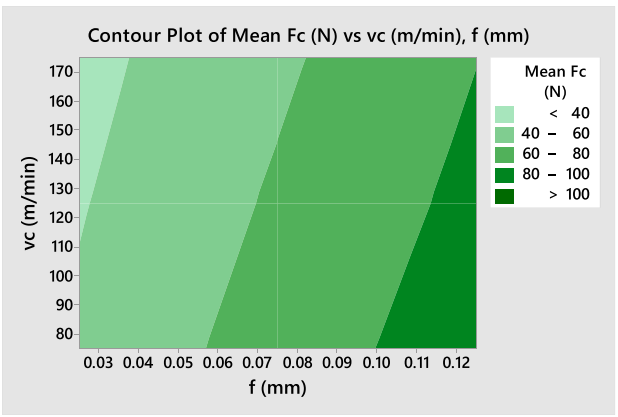

(a)

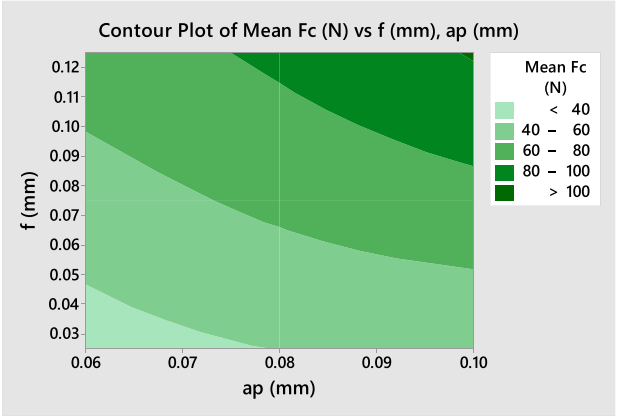

(b)

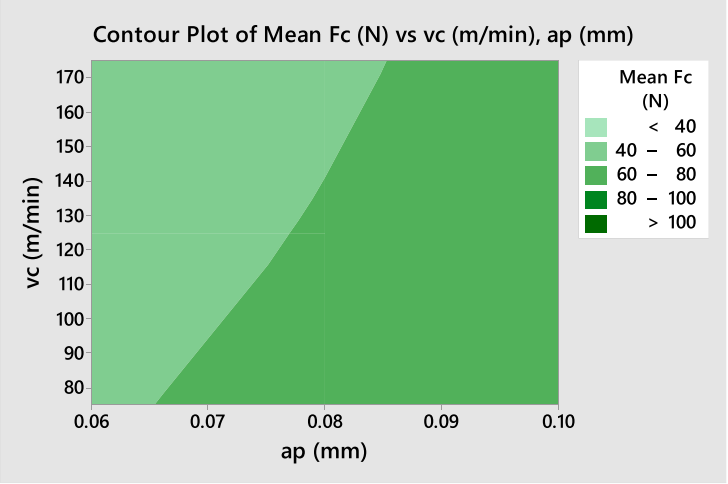

(c)

Fig. 4. Contour plot F_c with all process parameters.

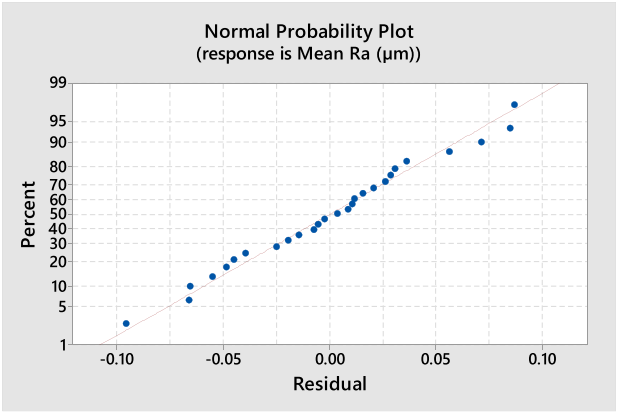

(a)

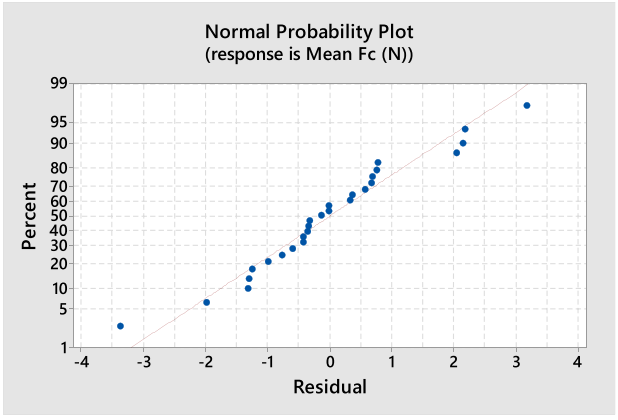

(b)

Fig. 5. Normal probability plots for (a) R_a and (b) F_c.

the Normal Probability Plots for R_a and F_c are shown in Fig. 5(a) and (b), respectively, along with 95 % confidence intervals. From these graphs, it is noticeable that when the experimental result gets closer to unity, it gets better and more in line with the model. The mathematical model in Equations (1) and (2) links the output response with the input machining parameters and serves as the objective function for a GA to get an optimal result.

$$\text{Surface roughness } (R_a) = 0.839–0.00258*v_c – 6.72*f – 10.4*a_p + 0.000010*v_c*v_c + 49.20*f*f + 40.8*a_p*a_p + 0.0129*v_c*f + 0.0164*v_c*a_p + 82.5*f*a_p – 0.425*v_c*f*a_p \quad (1)$$

$$\text{Cutting force } (F_c) = -5.2 + 0.026*v_c + 357*f + 695*a_p + 0.000087*v_c*v_c – 262*f*f – 1667*a_p*a_p – 1.77*v_c*f–1.77*v_c*a_p + 2141*f*a_p + 19.6*v_c*f*a_p, \quad (2)$$

where v_c is cutting speed, f is feed, and a_p is depth of cut.

3.2.2. GA approach for process parameters training and optimization

The multi-objective hybrid GA-RSM was used in this work as the best method in MATLAB 2019a. The regression mathematical equations (Equation (1) and Equation (2)) have been loaded into the fitness function in order to train and optimize the R_a and F_c using GA. The optimum fitness value is produced by varying the GA parameter functions throughout a series of trials. The parameter functions and values used in this GA process are listed in Table 7.

The genetic algorithm took just 450 rounds with 0.0632467 average spread to produce the most optimal result, which is a short amount of time. Fig. 6 depicts the Pareto front and the Average spread in each generation as a function of the number of repeats, and the input factors have been adjusted to produce the best feasible R_a and F_c. The optimal R_a and F_c with optimum input parameters for a multiobjective genetic algorithm in MATLAB 2019a were presented in Table 7. The pareto plot (Fig. 6) and Table 8 show that the goals are in competition (conflicting). It is difficult to accomplish both goals at once. A decision maker (a unit manager, engineer, or researcher) is provided the Pareto analysis results so they may choose a certain desirable point to run industrial HC. Other than what is offered in the Pareto solution, there are no superior points. It should be noted that the actual industrial working points (shown as solid squares) are not all perfect answers (hollow squares). The findings unequivocally demonstrate that it is feasible to increase a process' performance by only altering its operating conditions.

3.3. Multi-objective optimization of process response using hybrid Taguchi-GRA

3.3.1. Signal-to-noise ratio calculation

The signal-to-noise ratio (S/N ratio), which is also known as the ratio of the signal power to noise power, compares the strength of a desired signal to the strength of background noise. With the use of Minitab V5 and the greater is best option, the experimental findings of R_a and F_c were converted to S/N ratio and displayed in Table 9. The signal quality and noise level are both improved and reduced by a larger S/N ratio. The results of this S/N ration were used for optimization of the response outputs.

3.3.2. Normalization of measured data

The normalization of response values can be divided into three categories based on the intended use of the response values. When "the smaller the better" values are utilized, the initial normalization anticipates the objective function's lowest values. The second choice is "nominal the better," which averages the values of the goal function. The third one, "the larger the better," demands that the outputs be held to the highest standards. The smaller the better was selected for both R_a and F_c as the study's target function. Each output normalized values were calculated using Equation (3) and presented in Table 8 along with their results.

Table 7
GA parameter setting and its value.

Solver	Gamultobj
Population type	Double vectors
Population size	1000
Creation function	Feasible population
Fitness scaling function	Rank
Selection function	Tournament
Tournament size	4
Reproduction	Default values
Elite count	1.5 (0.05* Population size)
Crossover fraction	0.8
Mutation function	Adaptive feasible
Crossover function	Constraint dependent
Number of generations	600
Function tolerance	0.000001
Constraint tolerance	0.001

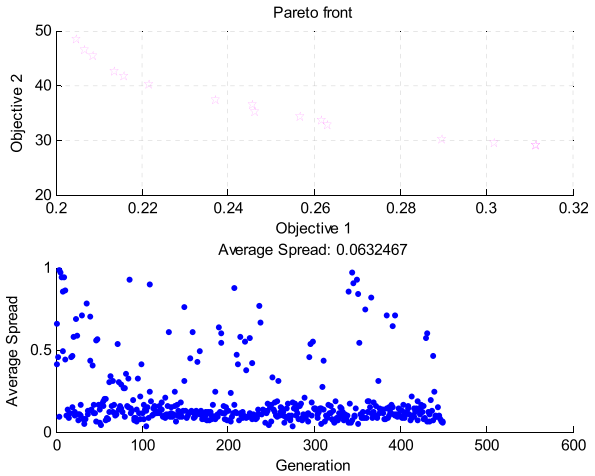

Fig. 6. Pareto front and Average spread as a function of iteration number.

Table 8
Pareto front - function values and decision variables.

S. No.	Cutting speed (m/min)	Feed (mm)	Depth of cut (mm)	R_a (μm)	F_c (N)
1	169.7410	0.0252	0.0629	0.3117	28.9407
2	87.2398	0.0250	0.0988	0.2049	48.4131
3	153.2423	0.0254	0.1000	0.2897	30.1230
4	163.2299	0.0255	0.0937	0.3019	29.5158
5	143.6495	0.0254	0.0906	0.2617	33.5675
6	169.7410	0.0252	0.0957	0.3117	28.9407
7	101.5176	0.0253	0.0696	0.2137	42.4982
8	104.2350	0.0250	0.0928	0.2086	45.3614
9	108.0809	0.0251	0.0991	0.2160	41.5965
10	124.3226	0.0251	0.0868	0.2463	35.0279
11	143.0133	0.0252	0.0916	0.2569	34.3204
12	136.5121	0.0252	0.0771	0.2631	32.7626
13	103.5338	0.0252	0.0899	0.2218	40.1075
14	130.5848	0.0252	0.0809	0.2371	37.2132
15	140.2040	0.0252	0.0629	0.2456	36.3228
16	98.1298	0.0253	0.0721	0.2069	46.5216

$$Z_{ij} = \frac{\boldsymbol{max}\left(\boldsymbol{y_{ij}}\right) - \boldsymbol{y_{ij}}}{\boldsymbol{max}\left(\boldsymbol{y_{ij}}\right) - \boldsymbol{min}\left(\boldsymbol{y_{ij}}\right)} \tag{3}$$

In this instance, i is equal to 1, 2, …, n, and j is equal to 1, 2, …, m, where m is the total quantity of responses studied and index n represents the number of experimental observations factors.

3.3.3. Grey relation coefficient (GRC) calculation

To describe the link between the ideal (best) and the actual normalized experimental outputs, the grey relational coefficient (GRC) is generated. The deviation sequences for the reference and comparability sequences were established before determining the grey coefficient. Equation (4) may be used to compute the deviation sequence ($\Delta_{oi}(k)$), which is then used to determine GRC. Their grades are provided in Table 8 following the processing of the data and the calculation of the GRC using Equation (5).

$$\Delta_{oi}(\boldsymbol{k}) = |\boldsymbol{y_o}(\boldsymbol{k}) - \boldsymbol{y_i}(\boldsymbol{k})|, \tag{4}$$

where $y_o(k)$ is the sequence and $y_j(k)$ is the comparability sequence.

$$\xi_i(\boldsymbol{k}) = \frac{\Delta_{min} + \xi\,\Delta_{max}}{\Delta_{oi}(\boldsymbol{k}) + \xi\,\Delta_{max}}, \tag{5}$$

where Δ_{min} and Δ_{max} are the minimum and maximum deviation sequences, respectively, and ξ is the distinguishing coefficient which equals 0.5.

Table 9
Response table for hybrid Taguchi-GRA.

S. No.	S/N ratio		Normalized Value		Grey relation coefficient (GRC)		GRG	Rank
	R_a	F_c	R_a	F_c	R_a	F_c		
			Smaller – the better	Smaller – the better				
Ideal Sequence			1.000	1.000	1.000	1.000		
1	−3.4785	37.6967	0.2220	0.2341	0.3913	0.3950	0.3931	22
2	−4.6717	36.2382	0.3157	0.3610	0.4222	0.4390	0.4306	19
3	−3.3626	36.8456	0.2130	0.3082	0.3885	0.4195	0.4040	20
4	−13.3917	30.1046	1.0000	0.8944	1.0000	0.8256	0.9128	1
5	−7.0719	33.2990	0.5040	0.6166	0.5020	0.5660	0.5340	12
6	−7.7655	33.9827	0.5585	0.5571	0.5311	0.5303	0.5307	13
7	−10.7820	28.8900	0.7952	1.0000	0.7094	1.0000	0.8547	2
8	−8.4732	35.0077	0.6140	0.4680	0.5643	0.4845	0.5244	15
9	−11.6672	30.9538	0.8647	0.8205	0.7870	0.7359	0.7614	4
10	−12.5418	31.2701	0.9333	0.7930	0.8823	0.7072	0.7948	3
11	−12.0760	31.9216	0.8967	0.7364	0.8288	0.6548	0.7418	6
12	−3.4011	38.2872	0.2160	0.1828	0.3894	0.3796	0.3845	23
13	−3.8088	37.8203	0.2480	0.2234	0.3994	0.3917	0.3955	21
14	−10.3425	36.0742	0.7607	0.3752	0.6763	0.4445	0.5604	11
15	−9.7356	36.9947	0.7131	0.2952	0.6354	0.4150	0.5252	14
16	−12.9950	33.0681	0.9689	0.6367	0.9414	0.5791	0.7603	5
17	−9.9788	35.1799	0.7322	0.4530	0.6512	0.4776	0.5644	10
18	−1.2396	39.2079	0.0463	0.1027	0.3440	0.3578	0.3509	26
19	−12.2167	32.9619	0.9078	0.6459	0.8443	0.5854	0.7148	8
20	−0.6490	40.3891	0.0000	0.0000	0.3333	0.3333	0.3333	27
21	−9.1186	37.3721	0.6647	0.2624	0.5986	0.4040	0.5013	18
22	−12.4685	34.0362	0.9275	0.5525	0.8734	0.5277	0.7006	9
23	−9.9515	37.9789	0.7300	0.2096	0.6494	0.3875	0.5184	16
24	−11.3727	31.7067	0.8416	0.7550	0.7594	0.6712	0.7153	7
25	−3.4655	40.3092	0.2210	0.0070	0.3909	0.3349	0.3629	25
26	−3.4011	39.6639	0.2160	0.0631	0.3894	0.3480	0.3687	24
27	−8.8739	36.4607	0.6455	0.3416	0.5851	0.4316	0.5084	17

3.3.4. GRG rank

The parameter approaches the optimum sequence as the GRC increases. The greatest multi-performance attribute is referenced by the high value of the GRC grade. Therefore, the best amount for each controllable element may be determined using the grey relational grade. By averaging the GRC for each performance feature, which are computed using Equation (6), the GRG is obtained.

$$\gamma_i = \frac{1}{n} \sum_{k=1}^{n} \xi_i(k), \tag{6}$$

where γ_i denotes the grey relational grade for the ith experiment and k is the number of performance characteristics.

In Table 8, the GRC are provided along with their grades. The multi-response properties are often better the higher the grey relational grade. The high precision CNC machine parameter setting of trial no. 4 produced the highest value of the GRG, as can be seen in Table 9. As a result, out of all 27 experiments, experiment 4 produces the greatest multi-performance characteristic. The average value for the GRG for each experimental trial level was presented in the response table (Table 10). A greater GRG is suggested by a better correlation between the two sequences since the GRG evaluates the degree of connection between the orientation and comparability orders. This has led to a greater value of GRG in the comparison sequence for the ultra-precision produced qualities under examination.

In this investigation, the levels with the largest average response were chosen based on this presumption. The greatest value of the GRG for the three control factors, A3, B1, and C1, respectively, may be seen in Table 9. In order to reduce R_a and F_c of the ultra-precision CBN turning of AISI D2, A3B1C1 represents the ideal combination of face turning parameters. It is also clear that the element linked to a high gain value has the greatest impact on the defining performance. It is obvious that control factor B has the greatest impact on performance. Fig. 7 illustrates the impact of each control component on the GRG, ensuring that the combination parameters used above were the best for maximizing the ultra-precision turning fabric characteristics under investigation.

Table 10
Response table for GRG.

Control Parameters	Symbol	Level - 1	Level - 2	Level - 3	Gain (Max-Min)
Cutting speed	A	0.540849	0.568137	0.57403[a]	0.033181
Feed	B	0.772938[a]	0.529686	0.380392	0.392545
Depth of cut	C	0.593969[a]	0.564193	0.524854	0.069115

Total average GRG = 0.56100514 a is the optimal level.

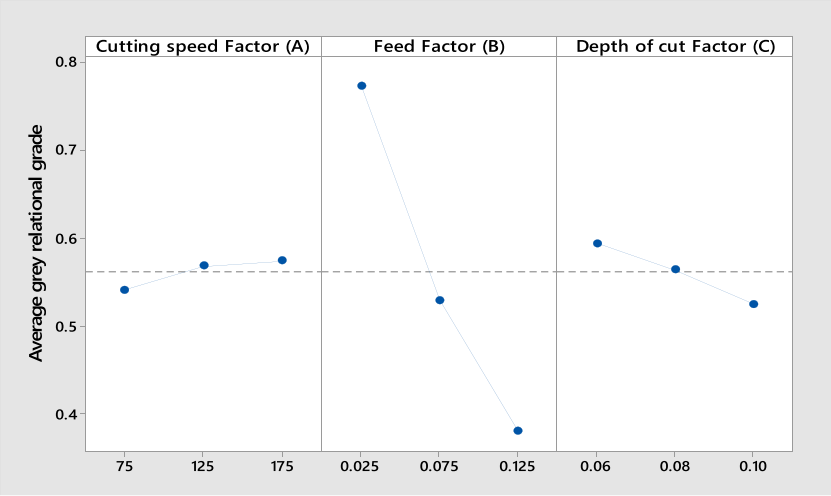

Fig. 7. Input factors and corresponding average GRG.

4. Conclusion

The impact of input parameters on the experimental outputs of surface roughness (Ra) and cutting force (Fc) was thoroughly investigated through Taguchi analysis, main effect plots, and contour plots. Results indicated that feed had the most significant influence on both Ra and Fc, followed by the depth of cut and cutting speed. Contour plots revealed that lower Ra values were achieved with lower feed rates, while cutting speed had a negligible effect. Similarly, Fc was notably affected by feed and cutting speed, with lower values obtained at lower feed rates and higher cutting speeds. These findings underscored the critical role of input parameters in shaping machining outcomes, emphasizing the importance of optimizing these parameters for improved performance.

Moreover, a multi-objective optimization approach utilizing a hybrid genetic algorithm-response surface methodology (GA-RSM) was employed to further enhance process responses. Regression models were developed to establish the relationship between machining parameters and Ra as well as Fc. The GA approach effectively trained and optimized Ra and Fc, yielding optimal results within a short timeframe. However, the Pareto analysis revealed conflicting goals, highlighting the challenge of simultaneously optimizing Ra and Fc. Decision-makers were provided with Pareto solutions to select desirable operating points for industrial applications, acknowledging the trade-offs between competing objectives.

Furthermore, a hybrid Taguchi-grey relational analysis (GRA) method was employed for multi-objective optimization. Signal-to-noise ratios were calculated to assess the quality of experimental data, which were then normalized for analysis. Grey relational coefficients were computed to evaluate the relationship between ideal and actual outputs, with higher coefficients indicating better performance. The grey relational grade (GRG) was utilized to identify the optimal combination of control factors for minimizing Ra and Fc in ultra-precision CBN turning. Control factor B emerged as the most influential, underscoring its importance in defining machining performance. Overall, these optimization techniques offered valuable insights into improving machining processes, highlighting the significance of parameter selection in achieving desired outcomes.

CRediT authorship contribution statement

Amanuel Diriba Tura: Writing – review & editing, Writing – original draft, Visualization, Validation, Software, Methodology, Investigation, Conceptualization. **Elly Ogutu Isaya:** Visualization, Validation, Software, Formal analysis, Data curation, Conceptualization. **Ugonna Loveday Adizue:** Visualization, Validation, Software, Resources, Data curation. **Balázs Zsolt Farkas:** Visualization, Validation, Supervision, Software, Project administration, Data curation. **Márton Takács:** Writing – review & editing, Visualization, Validation, Supervision, Project administration, Funding acquisition.

Declaration of competing interest

Amanuel Diriba Tura reports financial support was provided by Budapest University of Technology and Economics. Amanuel Diriba Tura reports financial support was provided by National Laboratory of Artificial Intelligence funded by the National Research, Development and Innovation Office (NRDIO) under the auspices of the Ministry for Innovation and Technology. Amanuel Diriba Tura reports financial support was provided by ED_18-2018-0006 (Research on prime exploitation of the potential provided by industrial digitalization). Amanuel Diriba Tura reports financial support was provided by the projects OTKA-K-132430 (Transient deformation, thermal and tribological processes at fine machining of metal surfaces of high hardness).

References

[1] S.J. Zhang, S. To, C.F. Cheung, H.T. Wang, Dynamic characteristics of an aerostatic bearing spindle and its influence on surface topography in ultra-precision diamond turning Spindle rotor Tilting motion, Int. J. Mach. Tools Manuf. 62 (2012) 1–12.

[2] A.K. Khalil, W.S. Yip, S. To, Theoretical and experimental investigations of magnetic field assisted ultra-precision machining of titanium alloys, J. Mater. Process. Tech. 300 (May 2021) (2022).

[3] A. Sharma, D. Datta, R. Balasubramaniam, Prediction of tool wear constants for diamond turn machining of CuBe, Journal of Micromanufacturing 4 (1) (Jul. 2020) 18–26, https://doi.org/10.1177/2516598420930992.

[4] L.N. Abdulkadir, K. Abou-El-Hossein, A.I. Jumare, P.B. Odedeyi, M.M. Liman, T.A. Olaniyan, Ultra-precision diamond turning of optical silicon—a review, Int. J. Adv. Des. Manuf. Technol. 96 (1–4) (Jan. 2018) 173–208, https://doi.org/10.1007/s00170-017-1529-x.

[5] C. Cheng, Z. Wang, W. Hung, S.T.S. Bukkapatnam, R. Komanduri, Ultra-precision machining process dynamics and surface quality monitoring, Procedia Manuf. 1 (2015) 607–618.

[6] W. Xingjun, W. Liping, W. Wei, H. Linshan, Study on surface quality factors of 10B/Al composite in ultra-precision turning, Procedia CIRP 71 (2018) 75–78.

[7] S. Azami, K. Hiroshi, T. Tanabe, J. Yan, Y. Kakinuma, Experimental analysis of the surface integrity of single-crystal calcium fluoride caused by ultra-precision turning, Procedia CIRP 13 (2014) 225–229.

[8] K. Okuda, T. Tanaka, M. Nunobiki, Machinability of Magnesium alloy in ultra-precision diamond cutting, Mater. Sci. Forum 422 (419) (2003) 975–982.

[9] R. Geng, X. Yang, Q. Xie, W. Zhang, J. Kang, Y. Liang, Ultra-precision diamond turning of ZnSe ceramics : surface integrity and ductile regime machining mechanism, Infrared Phys. Technol. 115 (March) (2021) 103706.

[10] Yintian Xing, C. Li, Y. Liu, C. Yang, C. Xue, Fabrication of high-precision freeform surface on die steel by ultrasonic-assisted slow tool servo, Opt Express 29 (3) (2021) 3708–3723.

[11] M. Kuruc, T. Vopát, J. Moravčíková, J. Milde, The precision analysis of cutting edge preparation on CBN cutting inserts using rotary ultrasonic machining, Mater. Manuf. Process. 13 (10) (2022).

[12] J. Grandgirard, D. Poinsot, L. Krespi, J.P. Nénon, A.M. Cortesero, Costs of secondary parasitism in the facultative hyperparasitoid Pachycrepoideus dubius: does host size matter? Entomol. Exp. Appl. 103 (3) (2002) 239–248.

[13] C. Junyun, J.I.N. Tianye, T. Yongjun, Development of an ultrahard nanotwinned cBN micro tool for cutting hardened steel, Sci. China Technol. Sci. 59 (6) (2016) 876–881.

[14] N.E. Sizemore, M.L. Nogueira, N.P. Greis, M.A. Davies, Application of machine learning for improved surface quality classification in ultra-precision machining of germanium, J. Manuf. Syst. 65 (2022) 296–316. December 2021.

[15] W. Minghai, W. Ben, Z. Yaohui, Weakening of the anisotropy of surface roughness in ultra-precision turning of single-crystal silicon, Chinese J. Aeronaut. 28 (4) (2015) 1273–1280.

[16] R. Ji, et al., Effect of grain refinement on cutting force of difficult-to-cut metals in ultra-precision machining, Chinese J. Aeronaut. 35 (2022) 484–493.

[17] H. Geng, D. Wu, H. Wang, Experimental and simulation study of material removal behavior in ultra-precision turning of magnesium aluminate spinel (MgAl 2 O 4), J. Manuf. Process. 82 (August) (2022) 36–50.

[18] P.A. McKeown, W.J. Wills-Moren, R.F.J. Read, H. Modjarrad, The design and development of a large ultra-precision cnc diamond turning machine, Advanced Manufacturing Processes 1 (1) (Jan. 1986) 133–157.

[19] S. Hate, K. Abou-el-hossein, Experimental investigation on the effects of magnetic fi eld assistance on the quality of surface fi nish for sustainable manufacturing of ultra-precision single-point diamond turning of titanium alloys, Front. Mech. Eng. (November) (2022) 1–14.

[20] C. Zhao, C.F. Cheung, An investigation of the cutting strategy for the machining of polar microstructures used in ultra-precision machining optical precision measurement, Micromachines 12 (755) (2021).

[21] X. Ruibin, H. Wu, Study on cutting mechanism of Ti6Al4V in ultra-precision machining, Int. J. Adv. Manuf. Technol. 10 (86) (2016) 1311–1317.

[22] H. Wang, S. To, C.Y. Chan, Investigation on the influence of tool-tip vibration on surface roughness and its representative measurement in ultra-precision diamond turning, Int. J. Mach. Tools Manuf. 69 (2013) 20–29.

[23] D. Wu, B. Wang, F. Fang, Effects of tool wear on surface micro-topography in ultra-precision turning, Int. J. Adv. Manuf. Technol. 102 (2019) 4397–4407.

[24] F. Schneider, R. Lohkamp, F.J.P. Sousa, R. Müller, J.C. Aurich, Analysis of the surface integrity in ultra-precision cutting of cp- titanium by investigating the chip formation, Procedia CIRP 13 (2014) 55–60.

[25] N. Kwak, J. Kim, D. Park, A research on ultra precision machining for Ti-6AL-4V alloy based biomedical applications using nano-positioning mechanism, J. Nano Res. 25 (2013) 157–173.

[26] M. Algarni, Mechanical properties and microstructure characterization of AISI 'D2' and 'O1' cold work tool steels, Metals 9 (1169) (2019) 1–10.

[27] J. Park, K. Kim, J. Kim, J. Jeon, Y. Koo, K. Lee, Microstructure and tensile properties of bulk AISI D2 tool steel fabricated by direct energy deposition, Mater. Charact. 194 (January) (2022) 112355.

[28] S. Deshwal, A. Td, I.F. Kumar, D. Chhabra, CIRP Journal of Manufacturing Science and Technology Exercising hybrid statistical tools GA-RSM , GA-ANN and GA-ANFIS to optimize FDM process parameters for tensile strength improvement, CIRP J. Manuf. Sci. Technol. 31 (2020) 189–199.

[29] H. Karimmaslak, B. Najafi, S.S. Band, S. Ardabili, F. Haghighat-Shoar, A. Mosavi, Optimization of performance and emission of compression ignition engine fueled with propylene glycol and biodiesel–diesel blends using artificial intelligence method of ANN-GA-RSM, Engineering Applications of Computational Fluid Mechanics 15 (1) (Jan. 2021) 413–425, https://doi.org/10.1080/19942060.2021.1880970.

[30] H. Ren, Z. Ma, W. Li, V. V Tyagi, A.K. Pandey, Optimisation of a renewable cooling and heating system using an integer-based genetic algorithm , response surface method and life cycle analysis, Energy Convers. Manag. 230 (2021) 113797.

[31] A.D. Tura, H.B. Mamo, D.G. Desisa, Multi-objective optimization and analysis for laser beam cutting of stainless steel (SS304) using hybrid statistical tools GA-RSM, IOP Conf. Ser. Mater. Sci. Eng. 1201 (1) (Nov. 2021) 12030.

[32] C.-M. Lin, Y.-T. Hung, C.-M. Tan, Hybrid taguchi–gray relation analysis method for design of metal powder injection-molded artificial knee joints with optimal powder concentration and volume shrinkage, Polymers 13 (6) (Mar. 2021) 865, https://doi.org/10.3390/polym13060865.

[33] R. Viswanathan, S. Ramesh, S. Maniraj, V. Subburam, Measurement and multi-response optimization of turning parameters for magnesium alloy using hybrid combination of Taguchi-GRA-PCA technique, Measurement 159 (2020) 107800.

[34] O.S. Onyekwere, M.H. Oladeinde, R.O. Edokpia, Multi-response optimization of bamboo fiber reinforced unsaturated polyester composites using hybrid taguchi – grey relational analysis method, J. Ind. Prod. Eng. 00 (00) (2020) 1–10.

[35] U.L. Adizue, A.D. Tura, E.O. Isaya, et al., Surface quality prediction by machine learning methods and process parameter optimization in ultra-precision machining of AISI D2 using CBN tool, Int. J. Adv. Manuf. Technol. 129 (2023) 1375–1394, https://doi.org/10.1007/s00170-023-12366-1.

[36] P. Protim, D. Shankar, Optimization of friction stir welding processes using hybrid-taguchi methods : a comparative analysis, Int. J. Interact. Des. Manuf. 17 (3) (2023) 1021–1038.

[37] M. Sheheryar, et al., Multi-objective optimization of process parameters during micro-milling of nickel-based alloy inconel 718 using taguchi-grey relation integrated approach, Materials 15 (23) (2022).

[38] B. Jiang, J. Huang, H. Ma, H. Zhao, H. Ji, Multi-objective optimization of process parameters in 6016 aluminum alloy hot stamping using taguchi-grey relational analysis, Materials 15 (23) (2022).

[39] A.A. Almetwally, Multi-objective optimization of woven fabric parameters using taguchi–grey relational analysis, J. Nat. Fibers 17 (10) (2020) 1468–1478.